Journal of Solid Mechanics Vol. 3, No. 3 (2011) pp. 244-257

Exact Solution for Electrothermoelastic Behaviors of a Radially Polarized FGPM Rotating Disk

A. Ghorbanpour Arani[1,*], A. Jafarzadeh Jazi[1], M. Abdollahian[1], M.R. Mozdianfard[2], M.Mohammadimehr[1], S. Amir[1]

[1]*Faculty of Mechanical Engineering, University of Kashan, Kashan, Islamic Republic of Iran*
[2]*Department of Chemical Engineering, Faculty of Engineering, University of Kashan, Kashan, Islamic Republic of Iran*

Received 3 July 2011; accepted 14 August 2011

ABSTRACT

This article presents an exact solution for an axisymmetric functionally graded piezoelectric (FGP) rotating disk with constant thickness subjected to an electric field and thermal gradient. All mechanical, thermal and piezoelectric properties except for Poisson's ratio are taken in the form of power functions in radial direction. After solving the heat transfer equation, first a symmetric distribution of temperature is produced. The gradient of displacement in axial direction is then obtained by assuming stress equation in axial direction to be zero. The electric potential gradient is attained by charge and electric displacement equations. Substituting these terms in the equations for the dimensionless stresses in the radial and circumferential directions yield these stresses and using them in the mechanical equilibrium equation a nonhomogeneous second order differential equation is produced that by solving it, the dimensionless displacement in radial direction can be achieved. The study results for a FGP rotating hollow disk are presented graphically in the form of distributions for displacement, stresses and electrical potential.

Keywords: Electrothermoelastic ; FGPM ; Radially polarized ;Rotating disk

1 INTRODUCTION

WITH advances of functionally graded piezoelectric material (FGPM) in industrial applications such as producing sensors and actuators, these materials have attracted much attention in recent years. Functionally graded materials (FGMs) are made of two material phases that has an intentional graded transition from one material at one surface to another material at the opposite surface; ceramics and metals are examples of these groups of materials. This transition allows the creations of multiple properties without implementing any mechanical interface. When a piezoelectric material is exposed to a stress field, electricity is produced due to polarization of material; apart from this, mechanical and thermal properties of FGPM are fairly similar to FGM. Galic and Horgan [1] presented a radially polarized piezoelectric cylinder under internal pressure. They presented an analytical solution to the axisymmetric problem of an infinitely long, radially polarized, radially orthotropic piezoelectric hollow circular cylinder. Chen et al. [2] studied the problem of a piezoceramic hollow sphere based on 3D equations of piezoelasticity. They investigated the effects of electroelastic field in a FGPM hollow sphere under mechanical and electric loading. Ding et al. [3] analyzed the dynamic responses of a functionally graded (FG) pyroelectric hollow sphere for spherically symmetric problems by solving a Volttera integral equation of the second kind using an interpolation polynomial to approximate the unknown function. They extended this problem for cylinder with plane strain assumption [4]. The exact solution for thermal-electro-elastic transient response in piezoelectric hollow

* Corresponding author. Tel.: +98 9131626594 ; Fax: +98 361 591 2424.
E-mail address: aghorban@kashanu.ac.ir (A. Ghorbanpour Arani).

structures was derived by Dai and Wang [5]. They showed that the response histories and distributions of stresses, electric displacement and electric potential interact with each other in a case of the transversely isotropic piezoelectric hollow sphere. Chen et al. [6] analyzed a FGPM hollow cylinder. They assumed that only the piezoelectric coefficient was varied quadratically in the radial direction while the other material parameters are assumed to be constant. The thermoelastic analysis of a FG rotating disk was presented by Hosseini Kordkheili and Naghdabadi [7], who investigated the influences of property gradation, centrifugal body loading and thermal loading on stresses and deformation. Bayat et al. [8] also studied the thermo elastic analysis of a FG rotating disk with small and large deflections. Later, they [9] investigated thermo elastic analysis for axisymmetric rotating disk made of FGM with variable thickness. Thermoelastic solution of a FG variable thickness rotating disk with bending based on the first-order shear deformation theory was also presented by Bayat et al. [10]. Oota and Tanigawa [11] studied the transient piezothermoelastic problem of a FG thermo-piezoelectric hollow sphere due to a uniform heat supply using the Laplace transformation method. Saadatfar and Razavi [12] investigated piezoelectric hollow cylinder with thermal gradient and used an analytical solution to the axisymmetric problem of a radially polarized, radially orthotropic piezoelectric hollow cylinder with thermal gradient. A 3D elasticity solution for FG rotating disks was also investigated by Asghari and Ghafoori [13] and suggested that although for the thin disks problems the 2D elasticity solution provided appropriate results, for the thick disks, a 3D elasticity solution should be used. Khoshgoftar et al. [14] studied thermoelastic analysis of a thick walled cylinder made of FGPM. They investigated the thermopiezoelectric behavior of a thick walled cylinder with FGM under the temperature gradient and inner and outer pressures. Hassani et al. [15] presented distributions of stress and strain components of rotating disks with non-uniform thickness and material properties subjected to thermo-elastic loading under different boundary conditions. Later they [16] investigated semi-exact solution for thermo-mechanical analysis of FG elastic-strain hardening rotating disks. Since rotating-disk systems are widely used in many industrial applications such as: aircraft engines, computer disk drivers, gas turbine engineering as fixed-free rotating disks and magnetic bearing systems as free-free rotating disks, therefore, investigation of rotating disks can be useful in designing such applications.

However, investigation into 3D solution for FGPM hollow rotating disk, placed in an electric field with a temperature gradient, has not been found in the literature. In this article, an analytical method is developed to determine stresses, displacement and electric potential fields. Initially, the heat transfer equation in the cylindrical coordinate system under inner and outer boundary conditions is solved in order to obtain the temperature distribution. Then, by substituting the electric displacement and temperature distribution in the dimensionless radial and circumferential stresses, theses stresses is obtained as a function of displacement. Finally, using equilibrium equation, and stress components, a displacement equation is presented which its solution at the corresponding boundary conditions yields the displacement, stresses components and electric potential.

2 TEMPERATURE DISTRIBUTION

Consider a FGPM rotating disk under electric, thermal and mechanical loadings Fig. 1. In this section, using the assumed boundary conditions, a solution is presented to the symmetric, steady state, heat transfer equation in the cylindrical coordinate system Eq. (1) as expressed by [2,14]:

$$\frac{1}{r}\left(rk(r)T'(r)\right)' = 0, \qquad (a \le r \le b) \tag{1}$$

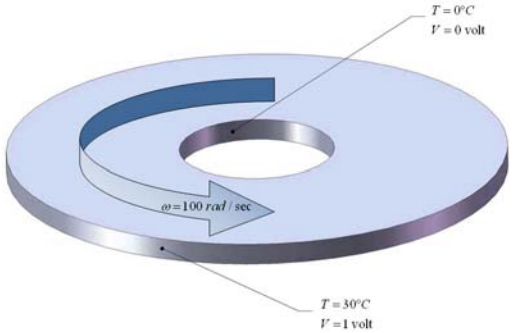

Fig. 1
Configuration of a radially polarized FGPM rotating disk.

where a and b are the inner and outer radii, respectively. Boundary conditions for Eq. (1) are defined according to [14, 17] as below:

$$Z_{11}T(a)+Z_{12}T'(a)=f_1 \tag{2a}$$
$$Z_{21}T(b)+Z_{22}T'(b)=f_2 \tag{2b}$$

In Eq. (2), $Z_{ij}(i=1,2;j=1,2)$ are the thermal constants which depend on the thermal conductivity and thermal convection. f_1 and f_2 are constants obtained at the inner and outer radii, respectively. $k(r)$ is assumed as a power function of r in Eq. (3):

$$k(r)=k_0 r^{\mu} \tag{3}$$

In which μ is a parameter indicating the nonhomogeneous extent of the material and k_0 is the nominal thermal conduction coefficient. Substituting Eq. (3) into Eq. (1) and integrating twice yields [2]:

$$T(r)=\frac{-Y_1}{\mu}r^{-\mu}+Y_2, \qquad (\mu\neq 0) \tag{4}$$

By assuming the defined boundary conditions Eqs. (2a), (2b), Y_1 and Y_2 constants in Eq. (4) are obtained as follows:

$$Y_1=\frac{Z_{21}f_1-Z_{11}f_2}{Z_{21}\left(Z_{12}a^{-(N+1)}-Z_{11}\dfrac{a^{-N}}{N}\right)-Z_{11}\left(Z_{22}b^{-(N+1)}-Z_{21}\dfrac{b^{-N}}{N}\right)} \tag{5a}$$

$$Y_2=\frac{f_2\left(Z_{12}a^{-(N+1)}-Z_{11}\dfrac{a^{-N}}{N}\right)-f_1\left(Z_{22}b^{-(N+1)}-Z_{21}\dfrac{b^{-N}}{N}\right)}{Z_{21}\left(Z_{12}a^{-(N+1)}-Z_{11}\dfrac{a^{-N}}{N}\right)-Z_{11}\left(Z_{22}b^{-(N+1)}-Z_{21}\dfrac{b^{-N}}{N}\right)} \tag{5b}$$

3 The GOVERNING EQUATION

The governing equation of a nonhomogeneous rotating disk is presented using a cylindrical system. The disk rotates about z axis with an angular velocity of ω. The axisymmetric aspect of the problem implies that shear stress components, $(\sigma_{r\theta},\sigma_{z\theta},u_{\theta})$ are negligible and assumed to be zero; similarly, $\partial/\partial\theta$ for all parameters are equal to zero. Also, since there is no stress in z direction, σ_{rz} and σ_{zz} are taken to be zero. Based on these assumptions, the constitutive relations could be expressed as follows [12, 18]:

$$\sigma_{rr}=c_{33}\varepsilon_{rr}+c_{13}\varepsilon_{\theta\theta}+c_{13}\varepsilon_{zz}+e_{33}\phi_{,r}-\lambda_1 T(r) \tag{6a}$$
$$\sigma_{\theta\theta}=c_{13}\varepsilon_{rr}+c_{11}\varepsilon_{\theta\theta}+c_{12}\varepsilon_{zz}+e_{31}\phi_{,r}-\lambda_2 T(r) \tag{6b}$$
$$\sigma_{zz}=c_{13}\varepsilon_{rr}+c_{12}\varepsilon_{\theta\theta}+c_{11}\varepsilon_{zz}+e_{31}\phi_{,r}-\lambda_3 T(r) \tag{6c}$$
$$D_{rr}=e_{33}\varepsilon_{rr}+e_{31}\varepsilon_{\theta\theta}+e_{31}\varepsilon_{zz}-\varepsilon_{33}\phi_{,r}-p_1 T(r) \tag{6d}$$

where [12, 13]:

$$\varepsilon_{rr}=\frac{\partial u_r}{\partial r},\qquad \varepsilon_{\theta\theta}=\frac{u_r}{r},\qquad \varepsilon_{zz}=\frac{\partial u_z}{\partial z}$$
$$\lambda_1=c_{33}\alpha_1+c_{13}\alpha_2+c_{13}\alpha_3,\ \lambda_2=c_{13}\alpha_1+c_{11}\alpha_2+c_{12}\alpha_3 \tag{7}$$
$$\lambda_3=c_{13}\alpha_1+c_{12}\alpha_2+c_{11}\alpha_3,\ p_1=e_{33}\alpha_1+e_{31}\alpha_2+e_{31}\alpha_3$$

In the above equations, $c_{ij}, e_{ij}, \alpha_{ij}, \varepsilon_{33}$ and p_1 are the elastic stiffnesses, piezoelectric constants, thermal expansion coefficients, dielectric constant and pyroelectric constant, respectively. Also, $\sigma_{ii}, \varepsilon_{ii}$ and D_{rr} represent stress, strain tensors and radial electric displacement, respectively. The equilibrium equation is as follows [7]:

$$\frac{\partial \sigma_{rr}}{\partial r}+\frac{\sigma_{rr}-\sigma_{\theta\theta}}{r}+\rho r\omega^2=0 \tag{8}$$

The charge equation of electro-statics without free charge density can be expressed [14] as follows:

$$div(D)=\frac{\partial (rD_{rr})}{r\partial r}=0\rightarrow\frac{\partial D_{rr}}{\partial r}+\frac{D_{rr}}{r}=0 \tag{9}$$

Since the stress component in z direction is zero, using Eq. (6c), displacement gradient in z direction is:

$$\sigma_{zz}=0\rightarrow\frac{\partial u_z}{\partial z}=-\frac{c_{13}}{c_{11}}\frac{\partial u_r}{\partial r}-\frac{c_{12}}{c_{11}}\frac{u_r}{r}-\frac{e_{31}}{c_{11}}\frac{\partial \phi}{\partial r}+\frac{\lambda_3}{c_{11}}T(r) \tag{10}$$

Substituting Eq. (10) into Eqs. (6a), (6b) and (6d) provides the radial and circumferential stresses as well as the electric displacement terms as follow:

$$\sigma_{rr}=\left(c_{33}-\frac{c_{13}^2}{c_{11}}\right)\frac{\partial u_r}{\partial r}+\left(c_{13}-\frac{c_{13}c_{12}}{c_{11}}\right)\frac{u}{r}+\left(e_{33}-\frac{c_{13}e_{33}}{c_{11}}\right)\frac{\partial \phi}{\partial r}-\left(\lambda_1-\frac{c_{13}\lambda_3}{c_{11}}\right)T(r) \tag{11a}$$
$$\sigma_{\theta\theta}=\left(c_{13}-\frac{c_{12}c_{13}}{c_{11}}\right)\frac{\partial u_r}{\partial r}+\left(c_{11}-\frac{c_{12}^2}{c_{11}}\right)\frac{u_r}{r}+\left(e_{31}-\frac{c_{12}e_{31}}{c_{11}}\right)\frac{\partial \phi}{\partial r}-\left(\lambda_2-\frac{c_{12}\lambda_3}{c_{11}}\right)T(r) \tag{11b}$$
$$D_{rr}=\left(e_{33}-\frac{e_{31}c_{13}}{c_{11}}\right)\frac{\partial u_r}{\partial r}+\left(e_{31}-\frac{e_{31}c_{12}}{c_{11}}\right)\frac{u_r}{r}-\left(\varepsilon_{33}+\frac{e_{31}^2}{c_{11}}\right)\frac{\partial \phi}{\partial r}-\left(p_1-\frac{e_{31}\lambda_3}{c_{11}}\right)T(r) \tag{11c}$$

In this work, the Poisson's ratio is considered as a constant while other material parameters such as elastic stiffnesses, piezoelectric constant, dielectric constant and thermal expansion coefficients are assumed to vary along the radial coordinate as bellow [4]:

$$c_{ij}=C_{ij}\left(\frac{r}{b}\right)^{\mu},\ (i,j=1,2,3),\qquad e_{3i}=E_{3i}\left(\frac{r}{b}\right)^{\mu}(i=1,3),$$
$$\varepsilon_{33}=\Omega_{33}\left(\frac{r}{b}\right)^{\mu},\ \rho=\rho_0\left(\frac{r}{b}\right)^{\mu},\ \mathrm{P}_1=p_1\left(\frac{r}{b}\right)^{2\mu},\ \Lambda_i=\lambda_i\left(\frac{r}{b}\right)^{2\mu} \tag{12}$$

where $C_{ij}, E_{3i}, \Lambda_i, \Omega_{33}, P_1$ and ρ_0 are known constants. To present the result, the following non-dimensional terms are introduced:

$$S=\frac{a}{b},\ \ u=\frac{u_r}{b},\ \ \sigma_r=\frac{\sigma_{rr}}{C_{33}-\frac{C_{13}^2}{C_{11}}},\ \ \sigma_\theta=\frac{\sigma_{\theta\theta}}{C_{33}-\frac{C_{13}^2}{C_{11}}},\ \ D_r=\frac{D_{rr}}{\sqrt{\left(C_{33}-\frac{C_{13}^2}{C_{11}}\right)\left(\Omega_{33}+\frac{E_{31}^2}{C_{33}}\right)}},\ \ A_1=\frac{C_{13}-\frac{C_{13}C_{12}}{C_{11}}}{C_{33}-\frac{C_{13}^2}{C_{11}}}$$

$$A_2=\frac{C_{11}-\frac{C_{12}^2}{C_{11}}}{C_{33}-\frac{C_{13}^2}{C_{11}}},\quad B_1=\frac{E_{33}-\frac{C_{13}E_{33}}{C_{11}}}{\sqrt{\left(C_{33}-\frac{C_{13}^2}{C_{11}}\right)\left(\Omega_{33}+\frac{E_{31}^2}{C_{33}}\right)}},\quad B_2=\frac{E_{31}-\frac{C_{13}E_{33}}{C_{11}}}{\sqrt{\left(C_{33}-\frac{C_{13}^2}{C_{11}}\right)\left(\Omega_{33}+\frac{E_{31}^2}{C_{33}}\right)}},\quad \Phi=\frac{\sqrt{\left(\Omega_{33}+\frac{E_{31}^2}{C_{33}}\right)}}{\sqrt{\left(C_{33}-\frac{C_{13}^2}{C_{11}}\right)}}\frac{\phi}{b}$$
$$T_1(\Upsilon)=\frac{\left(\Lambda_1-\frac{C_{13}\Lambda_3}{C_{11}}\right)T(r)}{\left(C_{33}-\frac{C_{13}^2}{C_{11}}\right)},\quad T_2(\Upsilon)=\frac{\left(\Lambda_2-\frac{C_{12}\Lambda_3}{C_{11}}\right)T(r)}{\left(C_{33}-\frac{C_{13}^2}{C_{11}}\right)},\quad T_3(\Upsilon)=\frac{\left(\mathrm{P}_1-\frac{E_{31}\Lambda_3}{C_{11}}\right)T(r)}{\sqrt{\left(C_{33}-\frac{C_{13}^2}{C_{11}}\right)\left(\Omega_{33}+\frac{E_{31}^2}{C_{33}}\right)}} \tag{13}$$

in which:

$$\Upsilon=\frac{r}{b} \tag{14}$$

Eqs. (4), (8), (9) and (11) can therefore be rewritten in the following form:

$$\sigma_r=\Upsilon^{\mu}\left[\frac{du}{d\Upsilon}+A_1\frac{u}{\Upsilon}+B_1\frac{\partial\Phi}{\partial\Upsilon}-\Upsilon^{\mu}T_1(R)\right] \tag{15a}$$
$$\sigma_\theta=\Upsilon^{\mu}\left[A_1\frac{du}{d\Upsilon}+A_2\frac{u}{\Upsilon}+B_2\frac{d\Phi}{d\Upsilon}-\Upsilon^{\mu}T_2(R)\right] \tag{15b}$$
$$D_r=\Upsilon^{\mu}\left[B_1\frac{du}{d\Upsilon}+B_2\frac{u}{\Upsilon}-\frac{d\Phi}{d\Upsilon}-\Upsilon^{\mu}T_3(R)\right] \tag{15c}$$

and

$$\frac{d\sigma_r}{d\Upsilon}+\frac{\sigma_r-\sigma_\theta}{\Upsilon}+\frac{b^2\rho_0\omega^2}{C_{33}-\frac{C_{13}^2}{C_{11}}}\Upsilon^{\mu+1}=0 \tag{16a}$$
$$\frac{dD_r(\Upsilon)}{d\Upsilon}+\frac{D_r(\Upsilon)}{\Upsilon}=0 \tag{16b}$$
$$T(\Upsilon)=\frac{-I_1}{\mu}\Upsilon^{-\mu}+I_2 \tag{17}$$

where I_1, I_2 are constants and can be obtained from the boundary conditions in Eq. (2). Using Eq. (16b), the following equation is obtained as

$$D_r(\Upsilon)=\frac{F}{\Upsilon} \tag{18}$$

where F is a constant. Substituting Eq. (18) into Eq. (15c) yields

$$\frac{d\Phi}{d\Upsilon}=B_1\frac{du}{d\Upsilon}+B_2\frac{u}{\Upsilon}-\Upsilon^{\mu}T_3(\Upsilon)-\frac{F}{\Upsilon^{\mu+1}} \tag{19}$$

Using Eqs. (19), (15a) and (15b) can be rewritten as:

$$\sigma_r=\Upsilon^{\mu}\left[G_1\frac{du}{d\Upsilon}+G_2\frac{u}{\Upsilon}-H_1(\Upsilon)\right]-\frac{G_4}{\Upsilon} \tag{20a}$$
$$\sigma_\theta=\Upsilon^{\mu}\left[G_2\frac{du}{d\Upsilon}+G_3\frac{u}{\Upsilon}-H_2(\Upsilon)\right]-\frac{G_5}{\Upsilon} \tag{20b}$$

where

$$G_1 = 1 + B_1^2, \qquad G_2 = A_1 + B_1 B_2, \qquad G_3 = A_2 + B_2^2, \qquad G_4 = B_1 F, \qquad G_5 = B_2 F,$$
$$G_6 = \frac{b^2 \rho_0 \omega^2}{C_{33} - \dfrac{C_{13}^2}{C_{11}}}, \qquad H_i(\Upsilon) = B_i T_3(\Upsilon) + T_i(\Upsilon)(i = 1,2) \tag{21}$$

Substituting Eqs. (20a) and (20b) into Eq. (16a), the following differential equation is obtained as a function of nondimensional radial displacement:

$$G_1 \Upsilon^2 \frac{\mathrm{d}^2 u}{\mathrm{d}\Upsilon^2} + R_1 \Upsilon \frac{\mathrm{d}u}{\mathrm{d}\Upsilon} + R_2 u = R_3 \Upsilon^{2-\mu} \tag{22}$$

where

$$R_1 = G_1(\mu + 1),\ R_2 = NG_2 - G_3,$$
$$\frac{R_3}{\Upsilon^{\mu-2}} = \Upsilon^{\mu+1}(2\mu J_1 I_2 - (J_2 - J_1) I_2) - G_5 \Upsilon^{-\mu} - G_6 \Upsilon^3 + \Upsilon\left(-J_1 I_1 + \frac{(J_2 - J_1) I_1}{\mu}\right) \tag{23}$$

The solution to Eq. (22) can be written as

$$u(\Upsilon) = C_1 \Upsilon^{L_1} + C_2 \Upsilon^{L_2} + K_1 \Upsilon + K_2 \Upsilon^3 + K_3 \Upsilon^{-\mu} + K_4 \Upsilon^{\mu+1} \tag{24}$$

where C_1 and C_2 are constants which are obtained from the boundary conditions, and

$$L_{1,2} = \frac{\left(1 - \dfrac{X_1}{G_1}\right) \pm \sqrt{\left(\dfrac{X_1}{G_1} - 1\right)^2 - 4\left(\dfrac{X_2}{G_1}\right)}}{2}, \qquad K_1 = \frac{-J_1 I_1 + \dfrac{(J_2 - J_1)}{\mu} I_1}{R_1 + R_2},$$
$$K_2 = \frac{-G_6}{6G_1 + 3R_1 + R_2}, \qquad K_3 = \frac{-G_5}{G_1 \mu(\mu+1) - \mu R_1 + R_2}, \qquad K_4 = \frac{2\mu J_1 I_2 - (J_2 - J_1) I_2}{G_1 \mu(\mu+1) + R_1(\mu+1) + R_2} \tag{25}$$

where

$$J_1 = \frac{B_1\left(P_1 - \dfrac{\Lambda_3 E_{33}}{C_{11}}\right)}{\left(C_{33} - \dfrac{C_{13}^2}{C_{11}}\right)\left(E_{33} - \dfrac{C_{13} E_{33}}{C_{11}}\right)} + \frac{\left(\Lambda_1 - \dfrac{C_{13}\Lambda_3}{C_{11}}\right)}{\left(C_{33} - \dfrac{C_{13}^2}{C_{11}}\right)}, \qquad J_2 = \frac{B_2\left(P_1 - \dfrac{\Lambda_3 E_{33}}{C_{11}}\right)}{\left(C_{33} - \dfrac{C_{13}^2}{C_{11}}\right)\left(E_{33} - \dfrac{C_{13} E_{33}}{C_{11}}\right)} + \frac{\left(\Lambda_2 - \dfrac{C_{12}\Lambda_3}{C_{11}}\right)}{\left(C_{33} - \dfrac{C_{13}^2}{C_{11}}\right)} \tag{26}$$

The electrostatic potential is obtained from Eq. (19)

$$\Phi = M_1 \Upsilon^{L_1} + M_2 \Upsilon^{L_2} + M_3 \Upsilon + M_4 \Upsilon^3 + M_5 \Upsilon^{-\mu} + M_6 \Upsilon^{\mu+1} + q \tag{27}$$

where q is constant and:

$$M_1 = C_1\left(\frac{B_2}{L_1}+B_1\right),\ \ M_2 = C_2\left(\frac{B_2}{L_2}+B_1\right),,\ \ M_3 = K_1(B_1+B_2)+\frac{I_1}{\mu}\frac{\left(\mathrm{P}_1-\frac{E_{31}\Lambda_3}{C_{11}}\right)}{\sqrt{\left(C_{33}-\frac{C_{13}^2}{C_{11}}\right)\left(\Omega_{33}+\frac{E_{31}^2}{C_{33}}\right)}},$$
$$M_4 = K_2\left(B_1+\frac{B_2}{3}\right),,\ \ M_5 = K_3\left(B_1-\frac{B_2}{\mu}\right)+\frac{F}{\mu},,\ \ M_6 = -\frac{\left(\mathrm{P}_1-\frac{E_{31}\Lambda_3}{C_{11}}\right)I_2}{(\mu+1)\sqrt{\left(C_{33}-\frac{C_{13}^2}{C_{11}}\right)\left(\Omega_{33}+\frac{E_{31}^2}{C_{33}}\right)}}+K_4\left(B_1+\frac{B_2}{\mu+1}\right) \tag{28}$$

Then, Eqs. (20a) and (20b) can be rewritten as:

$$\sigma_r = M_8\Upsilon^{L_1-1+\mu}+M_9\Upsilon^{L_2-1+\mu}+M_{10}\Upsilon^{\mu}+M_{11}\Upsilon^{\mu+2}+M_{12}\Upsilon^{-1}+M_{13}\Upsilon^{2\mu}+M_{14} \tag{29a}$$
$$\sigma_\theta = M_{15}\Upsilon^{L_1-1+\mu}+M_{16}\Upsilon^{L_2-1+\mu}+M_{17}\Upsilon^{\mu}+M_{18}\Upsilon^{\mu+2}+M_{19}\Upsilon^{-1}+M_{20}\Upsilon^{2\mu}+M_{21} \tag{29b}$$

where

$$\begin{aligned}
&M_8 = C_1(G_1L_1+G_2),\ \ M_9 = C_2(G_1L_2+G_2),\ \ M_{10} = K_1(G_1+G_2)-J_1I_2,\ \ M_{11} = K_2(3G_1+G_2),\\
&M_{12} = K_3(-\mu G_1+G_2)-G_4,\ \ M_{13} = K_4(G_1(\mu+1)+G_2),\ \ M_{14} = \frac{J_1I_1}{\mu},\ \ M_{15} = C_1(G_2L_1+G_3),\\
&M_{16} = C_2(G_2L_2+G_3),\ \ M_{17} = K_1(G_2+G_3)-J_2I_2,\ \ M_{18} = K_2(3G_2+G_3),\ \ M_{19} = K_3(-\mu G_2+G_3)-G_5,\\
&M_{21} = \frac{J_2I_1}{\mu},\ \ M_{20} = K_4(G_2(\mu+1)+G_3)
\end{aligned} \tag{30}$$

4 STEPS OF APPLIED METHODS

The following steps have been developed for obtaining results:
1- The temperature distribution of the disk is produced by solving the heat transfer equation.
2- The gradient of displacement in axial direction is obtained by assuming stress equation in axial direction to be zero.
3- The dimensionless electric potential gradient is attained by dimensionless charge and electric displacement equations.
4- Dimensionless radial and circumferential stresses are gained in terms of dimensionless radial displacement by substituting the results achieved in steps 2 and 3.
5- A nonhomogeneous second order differential equation is produced by substituting dimensionless stresses in the mechanical equilibrium equation.
6- Dimensionless radial displacement is attained in terms of dimensionless radius of the disk by solving the differential equation.
7- Dimensionless stresses in radial and circumferential directions and the electrostatic potential are obtained.

5 NUMERICAL RESULTS AND DISCUSSION

Table 1. presented the PZT4 material properties as FGPM material for analysis of the rotating disk [12, 18]. von-Mises stress for cylindrical coordinate system is considered as

$$\sigma_V = \sqrt{{\sigma_r}^2+{\sigma_\theta}^2-\sigma_r\sigma_\theta} \tag{31}$$

Table 1
Mechanical and electrical properties of PZT_4

C_{11}	139 (GPA)	α_1	2×10^{-5} (K^{-1})	E_{31}	-5.2 (c/m^2)	b	0.1 (m)
C_{12}	77.8 (GPA)	α_2	2×10^{-5} (K^{-1})	E_{33}	15.1 (c/m^2)	ρ_0	7500 (kg/m^3)
C_{13}	74.3 (GPA)	α_3	2×10^{-5} (K^{-1})	Ω_{33}	0.562×10^{-8} (c/Vm)	ω	100 (rad/sec)
C_{33}	115 (GPA)						

Numerical results are presented diagrammatically (see Figs. 2-11) in terms of dimensionless stresses, electric potential and displacement as a function of the rotating disks dimensionless radius from R=S to R=1. The boundary conditions for PZT4 are considered as two cases:

$$\text{case1 (free-free)}: \ \sigma_r(R=S)=0, \quad \sigma_r(R=1)=0, \quad \phi(R=S)=0, \quad \phi(R=1)=1 \tag{32a}$$

$$\text{case 2 (fixed-free)}: \ u(R=S)=0, \quad \sigma_r(R=1)=0, \quad \phi(R=S)=0, \quad \phi(R=1)=1 \tag{32b}$$

In both cases, the temperatures at inner and outer radii are $T_a=0°C$ and $T_b=30°C$, respectively. It should be noted that values of the nonhomogeneous extent (μ) considered in the diagrams presented here corresponds to 4 discrete numbers of -0.5, -0.25, 0.25 and 0.5; i.e. 2 positive and 2 negative values. Since μ exists in the denominators of the Eqs. (28) and (17), whenever μ takes the value of 0.0 or tends to a value very near it, there is no real solution for the problem as parameters such as stresses and electric potential tend to infinity. The comments made below regarding μ, corresponds only to the values mentioned above. The distribution of σ_r versus dimensionless radius of the disk for case 1 is presented in Fig. 2.Three major factors that increase the radial stress in this article are: piezoelectric reaction, centrifugal force and thermal gradient. For free-free boundary conditions, piezoelectric reaction and centrifugal force cause tension in the disk while thermal gradient cause compression in it. As can be seen σ_r is compressive, so temperature gradient is the dominant factor in the value of radial stress in the mentioned boundary conditions. Also the values of maximum dimensionless radial stress decrease with increasing μ and they tend toward higher values of R with increasing μ.

Fig. 3 shows the distribution of σ_r for fixed-free boundary conditions, i.e. case 2. Radial stress is compressive along the radius of the disk for fixed-free boundary conditions, too. It is observed from Fig. 3 that the values of radial stresses are decreased along the radius of the disk. Also the value of σ_r increases as μ is increased. Figs. 4 and 5 depict the distribution of σ_θ for both cases of boundary conditions discussed above (free-free and fixed-free, respectively). It is seen form Figs. 4 and 5 that σ_θ is compressive for inner layers of the disk, while for outer layers, σ_θ is tensile. Also, the values of σ_θ reduce with increasing μ for both cases. Figs. 6 and 7 show the dimensionless von-Mises stress (σ_V) distribution versus the dimensionless radius of the disk for cases 1 and 2, respectively. It is obvious form Figs. 6 and 7 that σ_V is decreased with increasing μ. Fig. 6 demonstrates that the minimum of σ_V takes place at the middle layers of the disk, while it is higher at inner and outer layers of the disk. Moreover, for case 2, as can be seen from Fig. 7, the maximum value of von-Mises stress takes place at outer layers of the rotating disk.

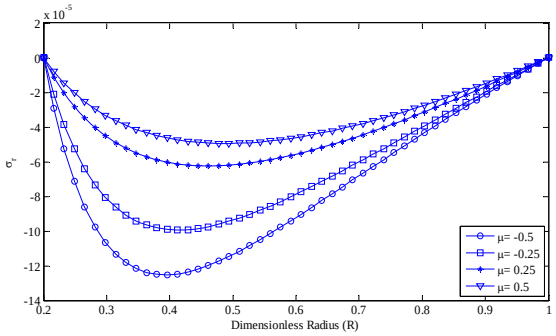

Fig. 2
Distribution of the dimensionless radial stress versus the dimensionless radius of the disk for free-free boundary conditions, $T_{in}=0°C$ and $T_{out}=30°C$.

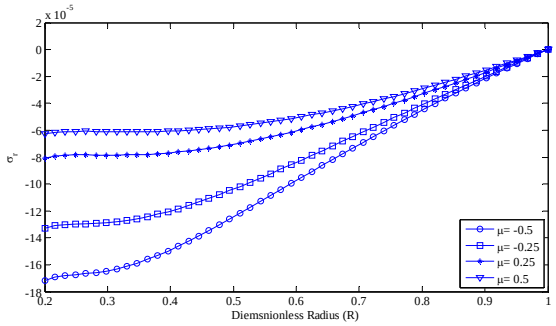

Fig. 3
Distribution of the dimensionless radial stress versus the dimensionless radius of the disk for fixed-free boundary conditions, $T_{in} = 0°C$ and $T_{out} = 30°C$.

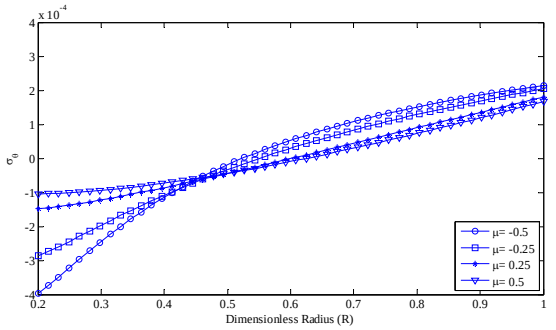

Fig. 4
Distribution of the dimensionless circumferential stress versus the dimensionless radius of the disk for free-free boundary conditions, $T_{in} = 0°C$ and $T_{out} = 30°C$.

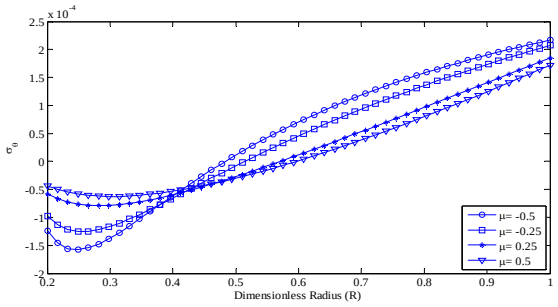

Fig. 5
Distribution of the dimensionless circumferential stress versus the dimensionless radius of the disk for fixed-free boundary conditions, $T_{in} = 0°C$ **and** $T_{out} = 30°C$.

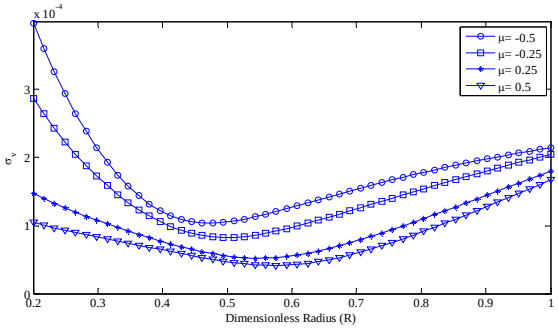

Fig. 6
Distribution of the dimensionless von Mises stress versus the dimensionless radius of the disk for free-free boundary conditions, $T_{in} = 0°C$ and $T_{out} = 30°C$.

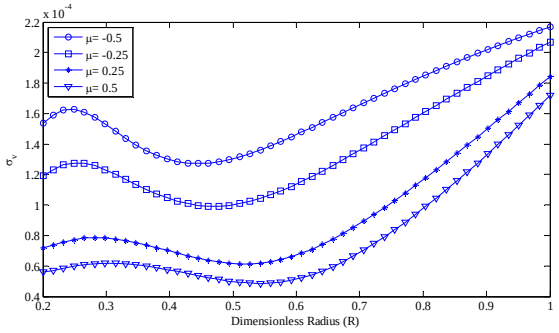

Fig. 7
Distribution of the dimensionless von Mises stress versus the dimensionless radius of the disk for fixed-free boundary conditions, $T_{in} = 0°C$ and $T_{out} = 30°C$.

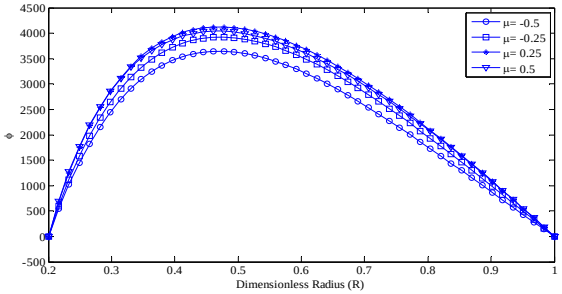

Fig. 8
Distribution of the electric potential versus the dimensionless radius of the disk for free-free boundary conditions, $T_{in} = 0°C$ and $T_{out} = 30°C$.

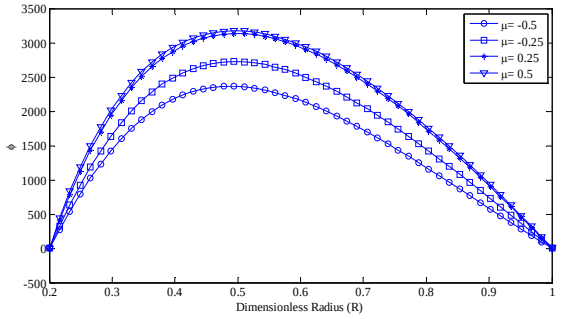

Fig. 9
Distribution of the electric potential versus the dimensionless radius of the disk for fixed-free boundary conditions, $T_{in} = 0°C$ and $T_{out} = 30°C$.

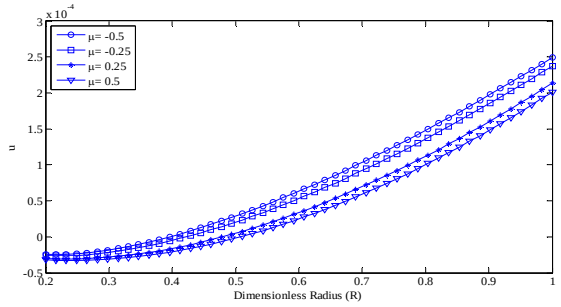

Fig. 10
Dimensionless radial displacement versus the dimensionless radius of the disk for free-free boundary conditions, $T_{in} = 0°C$ and $T_{out} = 30°C$.

The variations of the electric potential $(\phi(V))$ along the dimensionless radius of the disk are presented in Figs. 8 and 9 for cases 1 and 2, respectively. For both cases, the maximum value of ϕ increases as μ is increased. Also the maximum value of ϕ in case 1 is higher than those for case 2. In addition, it is observed from Figs. 8 and 9 that in

lower values of dimensionless radius, ϕ rises sharply up to R=0.48 and R=0.5 for cases 1 and 2 respectively, where a maximum is observed, before ϕ decreases slightly.

Figs. 10 and 11 illustrate the dimensionless radial displacement versus the dimensionless radius of the disk for cases 1 and 2, respectively. It is obvious form Figs. 10 and 11 that the dimensionless radial displacement is increased with increasing R for both cases; also it decreases as μ is increased. As can be seen form Fig. 10, the values of dimensionless radial displacement are negative at the inner surfaces of the disk. Therefore, the effect of thermal deformation is dominant rather than the deformation caused by rotation of the disk. In case 2, Figs 11 shows that the dimensionless radial displacement becomes negative especially for positive values of μ_0.

Figs. 12 and 13 indicate the effect of the temperature at inner radius of the disk on the dimensionless radial stress for free-free and fixed-free boundary conditions, respectively. As can be seen, the magnitude of dimensionless radial stress is increased by increasing the temperature at inner radius of the disk. Also increasing the temperature at inner radius of the disk has a similar effect on the dimensionless radial stress for both boundary conditions. In addition, the variation of the radial stresses is decreased with increasing the radius of the disk for both cases of boundary conditions. Figs. 14 and 15 show the effect of outer surface temperature on the dimensionless radial stress for both boundary conditions, free-free and fixed-free, respectively. The inner surface temperature is constant for all cases ($T_{in}=0°\text{C}$), four values are considered for outer surface temperature ($T_{out}=0,10,20,30°\text{C}$) and $\mu=-0.5$. In the case $T_{in}=T_{out}=0$, the radial stress caused by temperature equals to zero, and only piezoelectric and centrifugal effects cause radial stress in the disk. It is seen for two boundary conditions, that the first curves of these two figures are smaller than other curves, and the temperature is the dominant source of radial stress. Raising the outer surface temperature causes increase of the radial stress on the disk in pressure form. Also, the maximum value of dimensionless radial stress is greater in fixed-free boundary conditions.

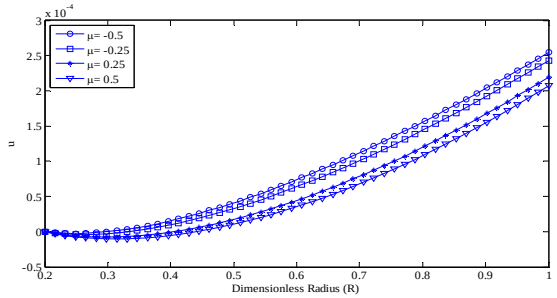

Fig. 11
Dimensionless radial displacement versus the dimensionless radius of the disk for fixed-free boundary conditions, $T_{in}=0°\text{C}$ and $T_{out}=30°\text{C}$.

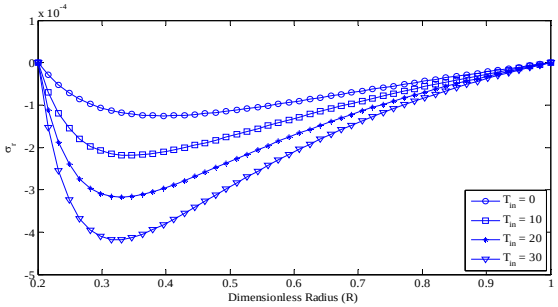

Fig. 12
Distribution of the dimensionless radial stress versus the dimensionless radius of the disk for free-free boundary condition, $T_{in}=0°\text{C}$ and $T_{out}=30°\text{C}$.

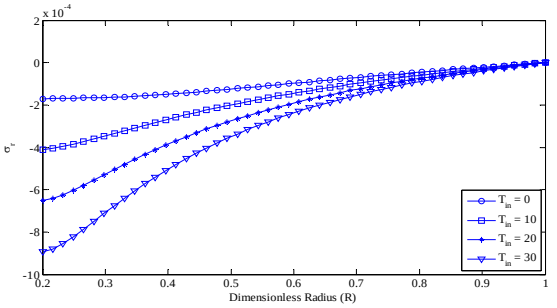

Fig. 13
Distribution of the dimensionless radial stress versus the dimensionless radius of the disk for fixed-free boundary condition, $T_{in}=0°\text{C}$ and $T_{out}=30°\text{C}$.

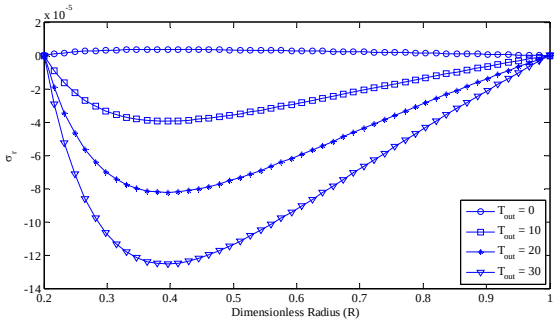

Fig. 14
Distribution of the dimensionless radial stress versus the dimensionless radius of the disk for free-free boundary condition, $T_{in} = 0°C$ and $T_{out} = 30°C$.

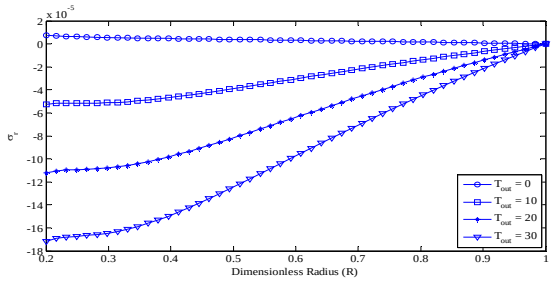

Fig. 15
Distribution of the dimensionless radial stress versus the dimensionless radius of the disk for fixed-free boundary condition, $T_{in} = 0°C$ and $T_{out} = 30°C$.

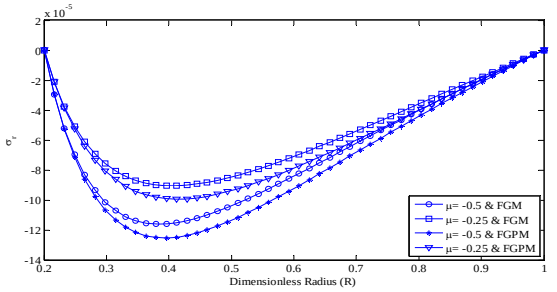

Fig. 16
Distribution of the dimensionless radial stress versus the dimensionless radius of the disk for free-free boundary condition, $T_{in} = 0°C$ and $T_{out} = 30°C$.

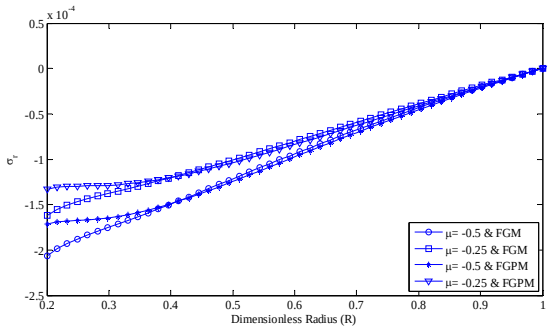

Fig. 17
Distribution of the dimensionless radial stress versus the dimensionless radius of the disk for fixed-free boundary condition, $T_{in} = 0°C$ and $T_{out} = 30°C$.

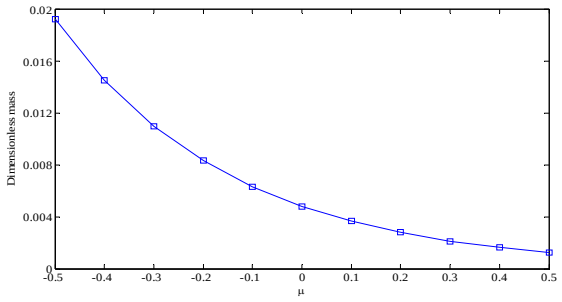

Fig. 18
Dimensionless mass of disk versus non-homogeneity parameter of the rotating disk.

Figs. 16 and 17 show the effect of piezoelectric properties on the dimensionless radial stress in the disk for free-free and fixed-free boundary conditions, respectively. Two non-homogeneity parameters are considered ($\mu = -0.5, -0.25$). The two first curve of each diagram are drawn for FGM disk (piezoelectric properties are vanished) and other two curves of each diagram are drawn for FGPM disk (piezoelectric properties are considered). As seen in Fig 16, the piezoelectric properties cause increase of pressure in the disk. In Fig 17, the piezoelectric properties have different effect; the negative radial stress is decreased until radius 0.4 but increased a bit after radius 0.4 for each non-homogeneity parameter. These effects show that imposed electric field on the FGPM disk causes negative radial strain. The effect of in-homogeneity parameter on the dimensionless mass and therefore, the weight of the rotating disk for PZT_4 is presented in Fig. 18. The following formulation is used to calculate the dimensionless mass of the rotating disk:

$$m = \int_{\forall} \rho \, d\forall = \int_a^b \rho(r) 2\pi r t dr = \frac{2\pi t \rho_0}{\mu+2} b^{\mu+2} \left(1 - (\frac{a}{b})^{\mu+2}\right) \Rightarrow \overline{m} = \frac{m}{2\pi t \rho_0} = \frac{b^{\mu+2}}{\mu+2}\left(1 - (\frac{a}{b})^{\mu+2}\right) \tag{33}$$

It is seen from Fig. 18 that the dimensionless mass and therefore the weight of the rotating disk decrease as μ is increased. Also it can be concluded from Eq. (33) that the value of dimensionless mass of the disk is independent from the material properties.

6 CONCLUSIONS

In this article, an exact solution was presented for a nonhomogeneous FGPM disk rotating about its axis at constant angular velocity, subjected to an electric field and thermal gradient in plane stress, using piezoelasticity theory. All mechanical, thermal and piezoelectric properties except for Poisson's ratio were taken in the form of continuous functions of dimensionless radius of the disk and are simulated in the form of power functions in radial direction.
Following presentation of the temperature distribution in the disk and assuming stress in z direction to be zero, the electric potential gradient was obtained by charge and electric displacement equations. Using the resulting stresses in radial and circumferential directions and the equilibrium equation, the displacement in radial direction was obtained. Dimensionless electro-thermo-mechanical stress distributions, displacement and electric potential curves for different values of in-homogeneity material parameter μ and inner and outer temperature and boundary conditions were drawn and discussed in details for a popular industrial piezocermaic material such as PZT_4. The following conclusions could be made from the dimensionless diagrams produced:

1. Distribution of stress, electric potential and electrical field can be controlled by selecting the FGPM material with appropriate mechanical and thermal properties.
2. The radial stresses for both free-free and fixed-free boundary conditions are compressive, which shows that stresses caused by thermal gradient are dominant.
3. Increasing the nonhomogeneous parameter μ considered for the discrete values studied here led to the reduction of value of radial and circumferential stresses and the radial displacement for both free-free and fixed-free boundary conditions.
4. Dimensionless von-Mises stresses decreased by increasing μ for both free-free and fixed-free boundary conditions.
5. The absolute values of all maximum ϕ's for free-free boundary conditions are higher than those for fixed-free boundary conditions.
6. Increasing the temperature of the inner and outer layers of the disk cause increasing the value of radial stresses for both free-free and fixed-free boundary conditions.
7. The values of dimensionless radial stresses of the disk increases considering the piezoelectric effect for free-free boundary conditions and it almost decreases for fixed-free boundary conditions.

ACKNOWLEDGMENTS

The authors would like to thank the referees for their valuable comments. They authors are also grateful to University of Kashan for supporting this work by Grant No. 65475/14.

REFERENCES

[1] Galic D., Horgan C.O., 2002, Internally pressurized radially polarized piezoelectric cylinders, *Journal of Elasticity* **66**: 257-272.

[2] Chen W.Q., Lu Y., Ye J.R, Cai J.B., 2002, 3D electroelastic fields in a functionally graded piezoceramic hollow sphere under mechanical and electric loading, *Archive of Applied Mechanics* **72**: 39-51.

[3] Ding H.J., Wang H.M.,Chen W.Q., 2003, Dynamic responses of a functionally graded pyroelectric hollow sphere for spherically symmetric problems, *International Journal of Mechanical Sciences* **45**: 1029-1051.

[4] Ding H.J., Wang H.M., Chen W.Q., 2004, Analytical solution of a special non-homogeneous pyroelectric cylinder for piezothermoelastic axisymmetric plane strain dynamic problems, *Applied Mathematics and Computation* **151**: 423-441.

[5] Dai H.L., Wang X., 2005, Thermo-electro-elastic transient responses in piezoelectric hollow structures, *International Journal of Solids and Structures* **42**: 1151-1171.

[6] Chen Y., Shi Z.F., 2005, Analysis of a functionally graded piezothermoelastic hollow cylinder, *J Zhejiang Univ SCI* **6A**: 956-961.

[7] Hosseini Kordkheili S.A., Naghdabadi R., 2007, Thermoelastic analysis of a functionally graded rotating disk, *Composite Structures* **79**: 508-516.

[8] Bayat M., Saleem M., Sahari B.B., Hamouda A.M.S., Mahdi E., 2007, Thermo elastic analysis of a functionally graded rotating disk with small and large deflections, *Thin-Wall Structures* **45**: 677-691.

[9] Bayat M., Sahari B.B., Saleem M., Hmouda A.M.S., Reddy J.N., 2009, Thermo elastic analysis of functionally graded rotating disks with temperature-dependent material properties: uniform and variable thickness, *International Journal of Mechanics and Mastererial Design* **5**: 263:279.

[10] Bayat M., Sahari B.B., Saleem M., Hmouda A.M.S., Wong S.V., Thermoelastic solution of a functionally graded variable thickness rotating disk with bending based on the first-order shear deformation theory, *Thin-Wall Structures* **47**: 568-582.

[11] Ootao Y., Tanigawa Y. 2007, Transient piezothermoelastic analysis for a functionally graded thermopiezoelectric hollow sphere, *Composite Structures* **81**: 540-549.

[12] Saadatfar M., Razavi A.S., 2009, Piezoelectric hollow cylinder with thermal gradient, *J Mech Sci Technol* **23**: 45-53.

[13] Asghari A., Ghafoori E., 2010, A three-dimensional elasticity solution for functionally graded rotating disks, *Composite Structures* **92**: 1092-1099.

[14] Khoshgoftar M.J., Ghorbanpour Arani A., Arefi M., 2009, Thermoelastic analysis of a thick walled cylinder made of functionally graded piezoelectric material, *Smart Materials and Structures* **18**: 115007.

[15] Hassani A., Hojjati M.H., Farrahi G., Alashti R.A., 2011, Semi-exact elastic solution for thermo-mechanical analysis of functionally graded rotating disks, *Composite Structures* **93**: 3239-3251.

[16] Hassani A., Hojjati M.H., Farrahi G., Alashti R.A., 2012, Semi-exact solution for thermo-mechanical analysis of functionally graded elastic-strain hardening rotating disks, **17**: 3747-3762.

[17] Jabbari M., Sobhanpour S., Eslami M.R., 2002, Mechanical and thermal stresses in a functionally graded hollow cylinder due to radially symmetric loads, *International Journal of Pressure Vessels and Piping* **79**: 493-497.

[18] Yang J., 2005, An introduction to the theory of piezoelectricity. Springer Science, Inc. Boston.